Fabrication of surface polymer brushes via thin film crystallization and solvent annealing

Jeffrey T. Wilk,[1] Andrew J. Chancellor,[2] Shan Mei,[1] Qian Qian,[1] Bin Zhao,[2,] and Christopher Y. Li[1,*]*

[1]Jeffrey T. Wilk, Dr. Shan Mei, Qian Qian, Prof. Christopher Li, Department of Materials Science and Engineering, Drexel University, Philadelphia, Pennsylvania 19104, United States

[2]Andrew J. Chancellor, Prof. Bin Zhao, Department of Chemistry, University of Tennessee, Knoxville, Tennessee 37996, United States

* Correspondence to: chrisli@drexel.edu (CYL); bzhao@utk.edu (BZ)

Abstract

Polymer single crystals have been used as templates to synthesize polymer brushes, known as the "polymer-single-crystal-assisted-grafting-to" (PSCAGT) approach. Polymer brushes with controlled grafting densities and spatial tethering locations have been demonstrated. Previous works focused on solution crystallization, which involves large amounts of organic solvent, and the grafting density can only be tuned by varying crystallization temperatures. In this work, thin film crystallization was utilized to fabricate two-dimensional (2D) polymer crystals on flat surfaces. Subsequent chemical tethering led to polymer brushes that retained the original morphology of the crystals with high fidelity. Furthermore, we show that the grafting density of the polymer brushes fabricated using this method depends on the chain end distribution on the top/bottom surfaces of the crystal, which can be facilely controlled by annealing the crystals at various nonsolvent media. Our work broadens the scope of the PSCAGT method and provides a new route to achieve polymer brushes with controlled structures.

1. Introduction

Polymer brushes, formed by end-tethered polymer chains onto flat or curved surfaces, have attracted significant interest due to their intriguing behaviors related to the stretched chain conformation and their capabilities to modify various solid surfaces.[1] Two synthetic approaches have been employed to fabricate polymer brushes: the grafting-to and grafting-from methods.[1a-c, 2] In the grafting-to approach, end-functionalized polymers are directly tethered onto surfaces to form a brush, while in the grafting-from method, initiators are first anchored onto a surface, followed by surface-initiated polymerization. Recent studies have shown that polymer single

crystals (PSCs) can be used as functional low dimensional nanomaterials, and several new potential applications of PSCs have been demonstrated.[3] These PSCs can guide nanoparticle assembly or ion transport.[4] Another interesting example is utilizing them as the 2D templates to synthesize surface polymer brushes, a new strategy called polymer-single-crystal-assisted grafting-to (PSCAGT).[5] In this method, end-functionalized polymers are first crystallized in a dilute solution into PSCs with the end functional groups on the crystal surfaces. Subsequent chemical coupling of these PSCs with solid substrates followed by washing leads to polymer brushes with precisely controlled morphology and grafting density. By utilizing telechelic chains, loop brushes with precisely controlled tethering points and sizes were synthesized, and they showed intriguing mechanical properties due to the Velcro-mimicking mechanism.[5c] Block copolymer brushes have also been fabricated using this approach.[5d] PSCs have also been used to synthesize Janus nanoparticles with compartmentalized polymer brushes.[6] Moreover, the programmed growth of PSC led to the formation of gradient brushes with the controlled spatial distribution of the brush grafting density.[5b] These examples demonstrate that PSCAGT is a versatile method to fabricate polymer brushes with controlled brush morphology.

The PSCs used in the previous PSCAGT approach are formed using solution crystallization. While solution crystallization affords clean PSCs with well-defined morphology, it is a rather time-consuming process with low yields and requires large amounts of organic solvents. In addition, attainable crystal shapes from solution crystallization are somewhat limited [3a, 7]. In recent years, work has been done to investigate polymer thin film crystallization, in which the polymer chain dynamics are significantly slowed down due to the small film thickness.[8] Various PSC shapes and geometries can be achieved by controlling the growth condition in thin film crystallization. For example, edge-on lamellae are often developed for

polymer films with a thickness greater than 100 nm. In contrast, flat-on lamellae are formed for thinner films due to the surface confinement effect.[8a] Crystallization in ultra-thin sub-10 nm films often leads to fractal crystal morphology due to the diffusion-limited crystal growth mechanism.[8a]

The rich morphology of thin film crystallization offers an opportunity of utilizing these thin film crystals as the template to synthesize surface polymer brushes following PSCAGT. Like the solution crystallization case, we anticipate that by crystallizing end-functionalized polymers in thin film followed by chemical tethering, controlled polymer brushes can be fabricated. For the development of brush structures using PSCAGT, flat-on morphology is desired as the crystal stem area density is maximized, thus promoting the contact of the end groups to the surface. In this work, we utilized triethoxysilane-end-functionalized poly(ε-caprolactone) (PCL-Si(OEt)$_3$) (number average molecular weight: 8.2 kDa, Đ: 1.07) as the model polymer because thin film crystallization of PCL has been systematically investigated [8a, 9] and PCL-Si(OEt)$_3$ has also been used to fabricate polymer brushes using solution crystallization-based PSCAGT.[5a] Detailed synthesis and characterization of the polymer are discussed in the supporting information (Scheme S1, Figures S1-S3). We show that well-defined PCL-Si(OEt)$_3$ single crystals can grow in a thin film under controlled conditions. These thin film crystals were then used as the template to fabricate PCL brushes. Single crystal morphology was retained in the brush state. More interestingly, the functional chain end distribution to the top/bottom crystal surfaces can be controlled by solvent annealing. A polar nonsolvent such as water pushes the -Si(OEt)$_3$ groups to the glass slide side in the crystal, leading to a higher grafting efficiency and a greater brush thickness. Our work demonstrates that combining the

newly developed PSCAGT with thin film crystallization and solvent annealing could lead to more versatile brush structures in surface polymer brushes.

2. Results and discussions

3.1 Polymer brushes fabricated by thin film crystallization in air.

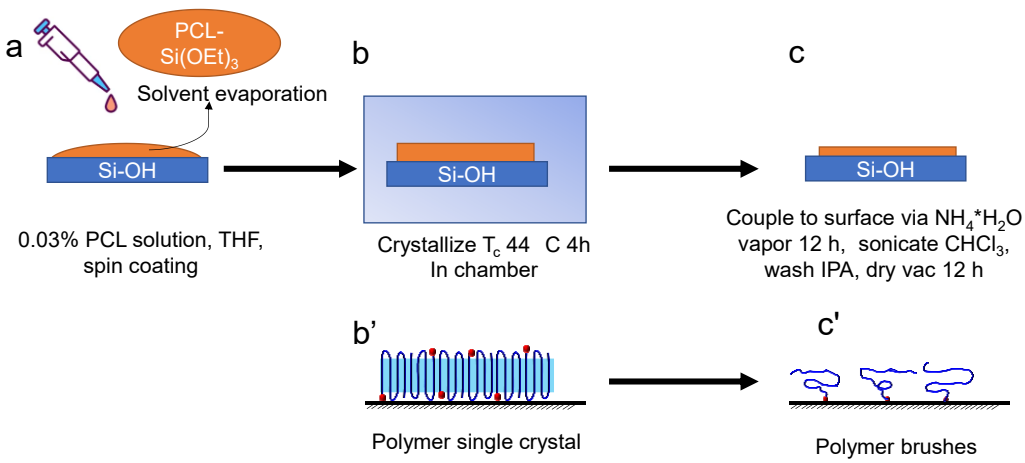

Scheme 1. The fabrication process of polymer brushes: (a) spin-coating a polymer solution onto a pre-cleaned glass slide, (b) thin film crystallization, (c) chemical tethering of the PSC onto the glass slide followed by washing. (b') and (c') show the schematics of the PSC and polymer brushes in (b) and (c).

Scheme 1 presents the fabrication procedure of polymer brushes using the thin film crystallization method. Polymer thin films were obtained by spin coating (Scheme 1a). The films were annealed at a pre-selected crystallization temperature (T_c) of 44 °C for 4 h (Scheme 1b). The T_c was chosen to be close to the melting temperature of the crystal, 50.27 °C based on the differential scanning calorimetry heating thermograms (Supporting information Figure S4). Afterward, the thin film crystals were chemically tethered onto the glass substrate, yielding desired polymer brushes. Different environments were applied in the crystallization/annealing

process, and the air-annealed crystal morphology was first examined through AFM imaging. The crystal morphology presents as 2D lamellae, shown in Figure a-c, with different magnifications. Flat and quasi-2D lamellar crystals are abundant in the figure. The average thickness is 8.3 ± 0.2 nm, and the lateral size of crystals is ~ 2-4 µm. While the local micro-facets are evidenced by the well-defined angles (indicated by white arrows in the figure), the crystals differ from the regular hexagon shape of PCL crystals obtained using solution crystallization.[5a] This morphological difference can be attributed to the confined diffusion of polymer chains on the glass substrate, which affects the growth kinetic of each crystalline plane.

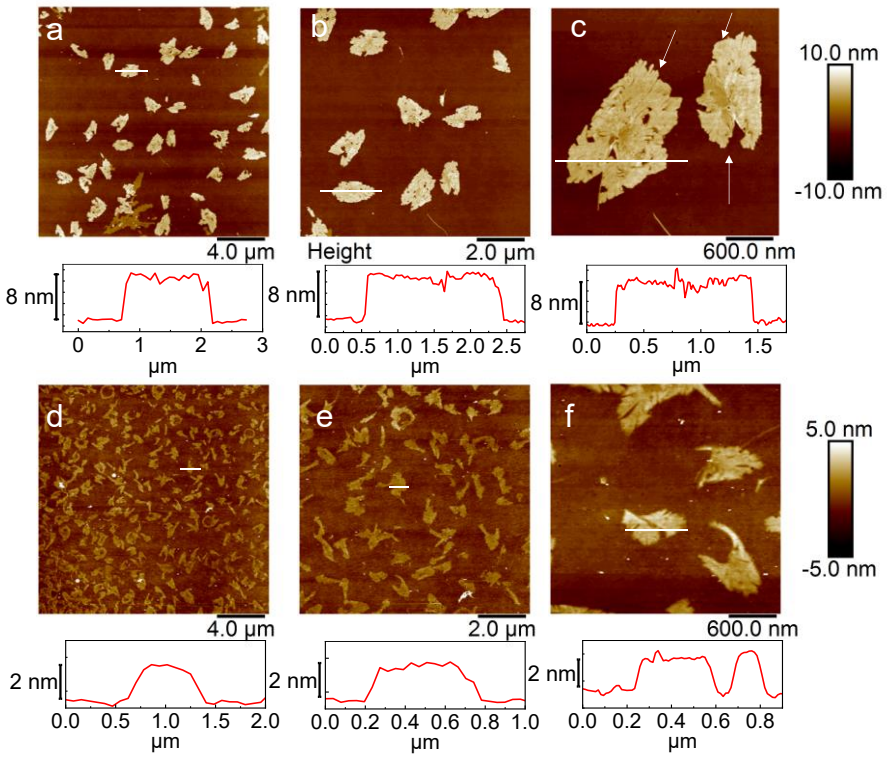

Figure 1: Crystal morphology of PCL annealed at 44 °C in air and the corresponding brush morphology from AFM imaging. (a-c) show the representative crystals at different magnifications after the annealing process and before tethering. The white horizontal lines correlate to the sampled height profile, shown below the images. (d-f) show the film after coupling the exposed triethoxysilane end groups to the surface silanol moieties on the glass slide and washing unbound polymer away, yielding tethered polymer brushes.

The air-annealed crystal samples were then exposed to an ammonia environment to assist the chemical tethering of the PSCs to the functionalized silanol glass slides via hydrolysis of the triethoxysilane end groups and condensation. After the surface reaction, the samples were washed in $CHCl_3$ to remove any unbound polymer chains on the glass surface. After drying in vacuum, the sample was re-examined by AFM to visualize any brush structures. As shown in Figures 1(d-f), the brush structures match the parent geometry of the preceding crystalline phase, albeit with lower thicknesses. The average brush thickness was measured by sectioning the brushes from the AFM topography scans, yielding an average height of 1.7 ± 0.2 nm.

The grafting density of the as-prepared brushes depends on the number of folds of the PCL chains in the crystal.[5a] This is because the folding of the PCL lamellae dictates the areal density of the triethoxysilane end group. The fold number, *n*, is calculated by considering the chain conformation of the PCL in the crystal (2_1 helix), orthorhombic lattice parameters of PCL (a = 0.747 nm, b = 0.498 nm, and c = 1.705 nm), [10] the degree of polymerization (DP) and the PSC height (h).

$$n = \frac{DP * c}{2 * h} - 1 \qquad (1)$$

Knowing the folding number of the PCL chain, the theoretical chain-end density, σ_t, can be calculated using equation (2), assuming the chain ends are evenly distributed on the two sides of the crystal.[5d]

$$\sigma_t = \frac{1}{(a * b)(n+1)} \qquad (2)$$

The experimental grafting density can be calculated from:

$$\sigma_{exp} = \frac{\rho \times h_b \times N_a}{MW} \qquad (3)$$

Where ρ is the polymer density (using 1.1 g cm^{-3}),[11] h_b is the polymer brush layer height, MW is the molar mass of the polymer brushes (DP × 114 g mol^{-1}), and N_a is the Avogadro's number.[5a]

The theoretical and experimental grafting density can be related using the coupling efficiency, shown in equation (4), which is the efficiency of the coupling reaction between the exposed triethoxysilane groups on the bottom face of the crystal and the substrate.[5a] A typical coupling scenario would yield a brush height of around one-half of the crystal height, as statistically, one-half of the end groups will be on the bottom surface towards the substrate, and the remaining chains being removed via washing with $CHCl_3$.

$$f = \frac{\sigma_{exp}}{\sigma_t} \times 100\% \qquad (4)$$

Based on this calculation, the chains fold approximately three times for the crystals annealed in air at 44 °C, having a height of 8.3 nm. The theoretical grafting density based on the statistical distribution of chain ends in the crystal, σ_t, is 0.63 chain nm^{-2}, with experimentally determined grafting density derived from brush height, σ_{exp}, being 0.25 chain nm^{-2}. This yields a grafting efficiency of 37.7%, which is likely due to both the efficiency of the coupling process and the deviation from a statistical distribution of chain ends upon the active silanol surface (see later discussion).

2.2 Polymer brushes fabricated by thin film crystallization in different environments

Equation 2 assumes an even distribution of the chain ends on the two sides of the crystal. The true polymer brush grafting density obtained from the PSCAGT method deviates from this theoretic value when the end group density of the crystal surface facing the substrate varies. It is reasonable to assume an even distribution of chain ends on the two surfaces of lamellar crystals obtained in solution crystallization. In contrast, in thin film crystallization, the substrate could

affect the chain end distribution in PSCs because the two sides of the PSCs are in contact with the substrate and air, respectively. This hypothesis is supported by a previous work demonstrating that 2D PCL crystals formed on the water surface have an asymmetrical, Janus-type structure with the polar -COOH end groups residing on one side of the crystals (water/PSC interface).[12] Scheme 2 shows two scenarios of polymer brushes formed by PSCs with similar thicknesses but different chain end locations. In Scheme 2a, approximately 50% of chain ends are located at the PSC/substrate interface, which can be chemically tethered onto the latter, while ~ 85% of the chain ends are located at the interface in Scheme 2b. One would anticipate that the grafting density in Scheme 2b is much higher. Solvent annealing has been extensively studied to increase local chain mobility and manipulate phase separation/crystallization in block copolymer and semicrystalline polymer thin films.[13] In this study, we introduce two non-solvents for the PCL-$Si(OEt)_3$ films, namely nonpolar hexane and polar water, to seek control of the polymer brush grafting density. It is anticipated that the spatial distribution of the -$Si(OEt)_3$ groups is dictated by their interaction with the glass substrate (bottom of the PSC) and the nonsolvent medium (top of the PSC).

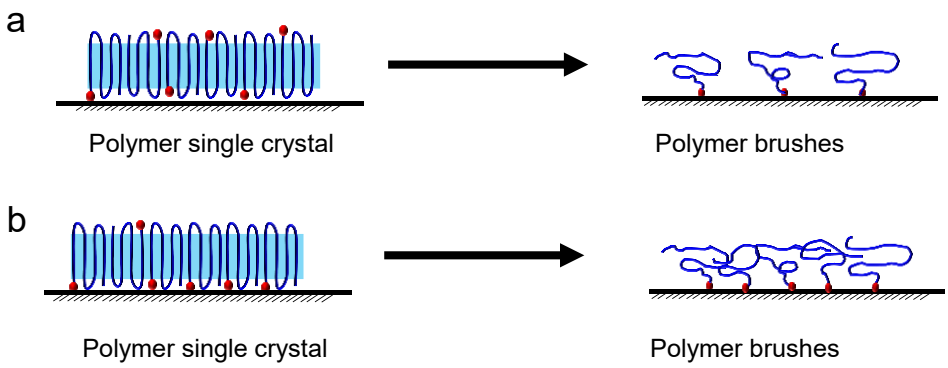

Scheme 2. Schematic representation of the effect of the chain end distribution on polymer brush grafting density. (a) Functional chain ends (red dots) are evenly distributed on the two sides of the single crystal. (b) Most functional chain ends are located on the single crystal/substrate interface. Brushes with a higher grafting density are obtained in (b).

To test the brush grafting efficiency derived from PSCs crystallized in a nonpolar environment, crystallization was conducted in hexane (Supporting information Scheme S2). Hexane is a nonsolvent for PCL, yet with higher compatibility with the methylene units in the PCL.[14] The annealed crystals, shown in Figure 2a, exhibit a faceted appearance with distinctive lateral growth. The edge of the crystals annealed in hexane show regions of thickening about the outer facet, which may be due to the increased freedom of the polymer chains near the crystal edges. The average height of the PSCs is ~ 8.3 nm ± 0.3 nm, like the air-annealed samples. The formed crystals were chemically tethered to the glass slides, and the unbound chains were washed away, yielding the brushes shown in Figure 2b. Like in the previous case, the brush state directly mimics the morphology of the parent crystalline state. The brush displays a measured height of 1.0 nm ± 0.2 nm, significantly lower than the previous air-annealing condition. This lower brush height indicates a reduced grafting density and a lower grafting efficiency compared to the air-annealed case, 0.15 chains nm^2 and 22.5%, respectively, obtained using equations (3) and (4). The reduction in brush height and, in turn, grafting density can provide clues about the state of the chain ends in PSCs from annealing in this nonpolar environment. The chemical tethering of the polymer chains depends on the proximity of the triethoxysilane end groups to the active silanol surface, facilitating the hydrolysis of the silane chain ends and the formation of -Si-O-Si- bonds with the substrate. The reduced brush height and lower grafting density/efficiency observed in the hexane-annealed samples suggest that the hexane nonsolvent environment reduces the silane end-group density on the crystal's bottom surface, lowering the grafting density.

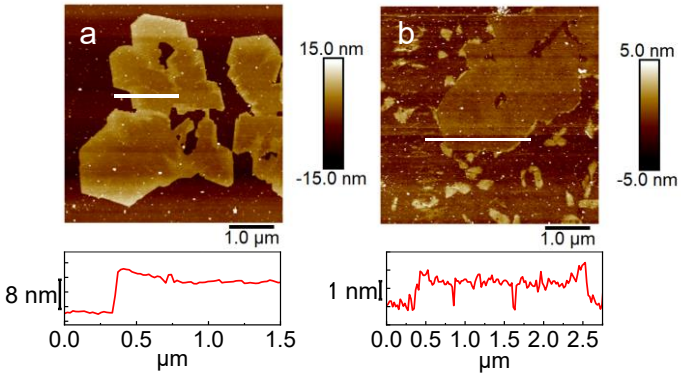

Figure 2. Crystal morphology of PCL annealed in hexane and corresponding brushes from AFM imaging. (a) Single crystals generated after spin-coating and annealing in hexane at 44 °C, and (b) the corresponding brush structures after tethering and removal of the unbound chains.

Polar nonsolvent H_2O was then used as the medium for polymer crystallization. Well-defined lamellar single crystals were observed over the entire surface, shown in Figure 3(a-b). The crystal morphology presents as a single or a cluster of leaf-shaped crystals. After the removal of untethered PCL chains, rich brush structures were revealed using AFM imaging, shown in Figure 3(c-d). The brush morphology replicates their parent crystal shapes, like the air- and hexane-annealed samples. The measured crystal height was 8.2 ± 0.3 nm. The average brush height was measured to be 2.4 ± 0.1 nm. This yields a grafting density of 0.35 chains nm^{-2} and a grafting efficiency of 53.9%, significantly higher than those of the hexane-annealed samples. The higher brush thickness, grafting density, and coupling efficiency suggest that the silane end group is encouraged to migrate toward the glass surface during annealing in a water environment and subsequently react with the surface silanol groups.

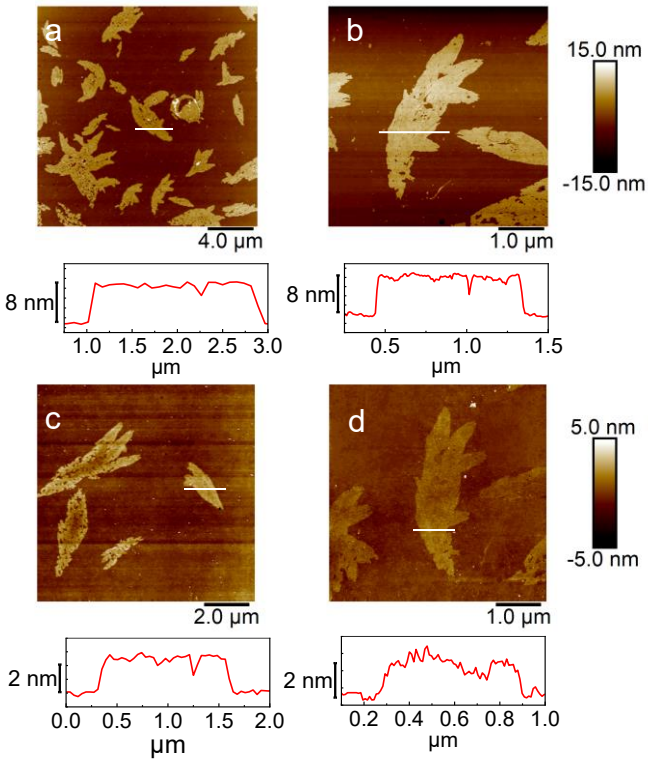

Figure 3: AFM height images of PCL crystals and corresponding brushes from annealing in polar, non-solvent water. The spin-coated samples were subjected to crystallization in water at T_c = 44 °C for 4 h. a-b) crystal morphology, c-d) brush morphology after washing in $CHCl_3$.

To further verify the annealing environment effect on the brush grafting density, as-prepared PCL films were also used as a control to fabricate polymer brushes. In this experiment, the PCL-Si(OEt)$_3$ solution was spin-cast onto a glass slide at 3000 RPM and then investigated under AFM without further annealing, shown in Figure 4. Despite the short timeframe during the removal of THF, PCL-Si(OEt)$_3$ could still form isolated single crystals with various shapes. The lamellar height of the crystals after evaporation was determined to be 8.0 ± 0.3 nm, slightly lower than the heights of PSCs formed via annealing. Upon removal of the unbound chains and the development of the brush structure, the brush height was determined to be 2.0 ± 0.2 nm, with a grafting density and a coupling efficiency of 0.29 chains nm^{-2} and 46.0%, respectively.

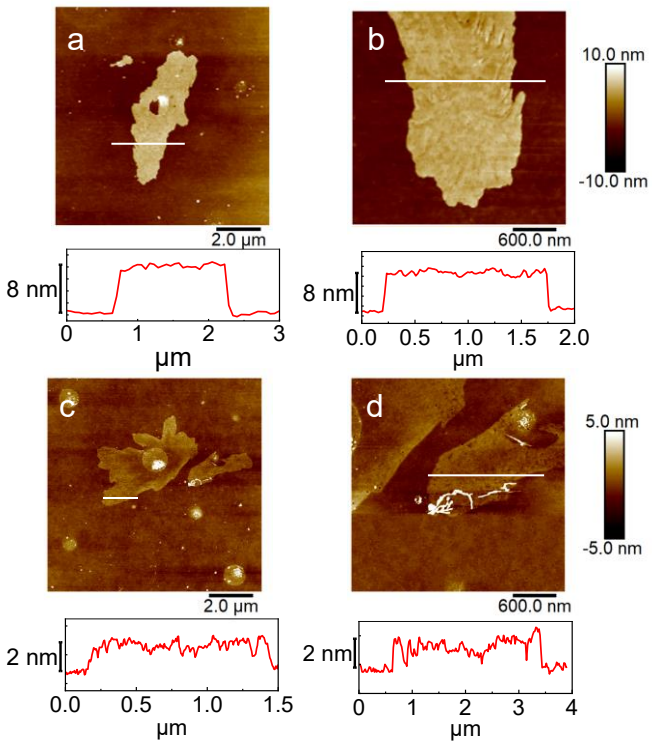

Figure 4. AFM height images of crystals and corresponding brushes from spin-coating of PCL-$Si(OEt)_3$ in THF. (a-b) crystal morphology after spin coating. (c-d) brush formation after the removal of unbound chains.

2.3. Discussion

The summary of the environmental conditions is tabulated below in Table 1, which shows that crystallization in air, hexane, and water produced PSCs with similar lamellar thickness. However, the resultant brush heights and the grafting densities are different. We can assume that the efficiency of the coupling reaction between each available triethoxysilane end group and the silanol surfaces is constant; the observed differences in grafting density are caused by the varied coupling efficiency, which would be solely due to the distribution and population of triethoxysilane end groups located on the active coupling surface. Both grafting density and grafting efficiency are plotted as a function of brush height following equations 3 and 4, shown in Figure 5. As the annealing environment varies from hexane to water, the polymer brush

height increases from 1.0 to 2.4 nm, and the grafting density increases from 0.15 to 0.35 chains/nm^2. This observation confirms that since the -Si(OEt)$_3$ chain end group is hydrophobic, as the crystallization environment becomes increasingly hydrophilic (from hexane to water), the -Si(OEt)$_3$ groups are pushed to the PSC-substrate interface during annealing, and the brush grafting density therefore increases.

The as-cast samples provide evidence on the environmental effect on the chain end distribution. Compared to the annealed samples, which were crystallized for 4 h, the as-cast samples were formed within 30 sec, and thus, the substrate/environment have a less significant effect on the chain end distribution. The rapid formation of the PSC crystalline phase acts as a kinetic quench due to the fast evaporation of THF during the spin coating process, hindering chain mobility. This sample yields a brush thickness of 2.0 ± 0.3 nm and a grafting density of 0.29 chains/nm^2, between the water-annealed and air-annealed samples. This suggests that even for air-annealed samples, the -Si(OEt)$_3$ chain ends are repelled away from the glass substrate, which is likely due to the high surface energy of the glass substrate. Note that for practical applications, complete coverage of the brushes on the substrate would be important, which could be achieved by optimizing the thickness of as-cast films or multi-step coating.

Table 1: Comparison of the crystals and brushes for different environmental annealing conditions

Condition	**T_c (°C)[1]**	**t_c (hr)[2]**	**H_c (nm)[3]**	**n**	**H_b (nm)[4]**	**σ_t (chains nm^{-2})**	**σ_{exp} (chains nm^{-2})**	**f (%)[5]**
Spin Coated	-	-	8.0 ± 0.3	3.3	2.0 ± 0.2	0.63	0.29	46.0
Annealing, Air	44	4	8.3 ± 0.2	3.1	1.7 ± 0.2	0.65	0.25	37.7
Annealing, H_2O	44	4	8.2 ± 0.3	3.2	2.4 ± 0.1	0.65	0.35	53.9
Annealing, C_6H_{14}	44	4	8.2 ± 0.3	3.1	1.0 ± 0.2	0.65	0.15	22.5

[1] *Crystallization temperature*
[2] *Crystallization Time*
[3] *Crystal Height*
[4] *Brush Height*
[5] *Grafting Efficiency*

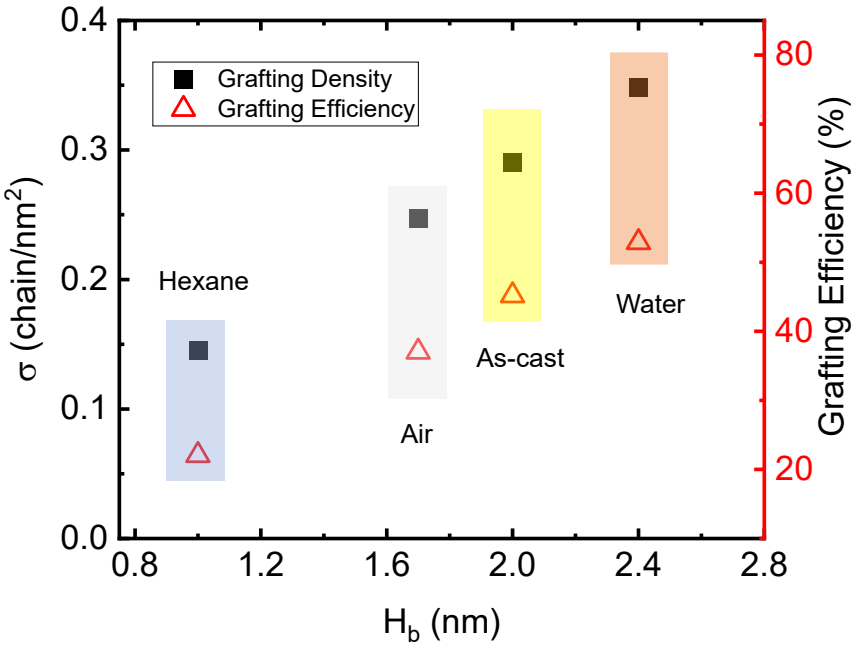

Figure 5. Comparison of grafting density and grafting efficiency for different environmental annealing conditions. The results highlight that the polymer brush grafting density can be facilely controlled by the annealing environment in the PSCAGT method.

3. Conclusions

In summary, this work demonstrated that thin film crystallization can be used in PSCAGT to synthesize polymer brushes. PCL-Si(OEt)$_3$ thin films were crystallized in different environments, and through PSCAGT, a series of polymer brushes with different brush heights, grafting density, and morphology was obtained. Solvent annealing was proven effective in

controlling the chain end distribution of the thin film crystals, which in turn dictated the brush thickness and grafting density. Polar water pushes the -Si(OEt)$_3$ group to the PSC/substrate interface, leading to a higher grafting density, while nonpolar hexane yields polymer brushes with the lowest grafting density. This work demonstrates a facile approach to fabricating polymer brushes with controlled morphology and grafting densities.

4. Experimental

Materials

Poly(ε-caprolactone) (PCL) with one end-functionalized with a triethoxysilane group (PCL-Si(OEt)$_3$) was used in this work. This polymer was synthesized by ring-opening polymerization of ε-caprolactone in toluene at 75 °C using 2-(2-methoxyethoxy)ethanol as initiator and tin(II) 2-ethylhexanoate as catalyst,[15] followed by the reaction of the hydroxyl chain end with (3-isocyanatopropyl)triethoxysilane in the presence of dibutyltin dilaurate. The degree of polymerization (DP) for the polymer precursor (PCL-OH) was 40 from the end group analysis via ^{1}H NMR spectroscopy, which was very close to the DP of 43 calculated from the monomer conversion, indicating that the polymerization was controlled. Size exclusion chromatography of PCL-Si(OEt)$_3$ showed that the $M_{n,SEC}$ was 8.2 kDa and the Đ was 1.07, relative to polystyrene standards. Detailed synthesis and characterization can be found in the Supporting Information. Tetrahydrofuran (THF, 99.9%, Aldrich) was dried over activated No. 3 molecular sieves before use. Isopropyl alcohol (IPA, 99%, Aldrich) was distilled over calcium hydride (CaH_2, Aldrich) before use. Chloroform ($CHCl_3$, 95%, Aldrich), hexane (C_6H_{14}, 97%,

Aldrich), deionized water (VWR) and ammonium hydroxide (NH_4 * H_2O) 30%, BDH) were used without further purification unless otherwise noted.

Fabrication of Crystalline Films

PCL-$Si(OEt)_3$ was dissolved in THF at 0.03 wt% and vortexed for 5 min at room temperature. Glass slides were etched using 4 : 1 H_2SO_4 : H_2O_2 ("piranha" solution) for 12 h, then washed with DI water and IPA, and stored in IPA for future use. 30 µL of the PCL solution was cast onto the "piranha"-etched glass slides and spun at 3000 RPM for 30 sec. PCL-$(SiOEt)_3$ films were then inserted into a solvent annealing chamber containing air (or water, or hexane) and allowed to anneal for 4 h at 44 °C, as shown in Scheme S2 in the Supporting Information. The films were lightly blotted dry with a nylon 6,6 filter paper before being dried under vacuum at room temperature for 12 h for further characterizations.

Fabrication of Polymer Brush Films

Crystallized PCL-$Si(OEt)_3$ films were placed in a sealed petri dish containing a 2 mL NH_4OH solution to react with the ammonia vapor for 12 h. After the reaction, the films were submersed in 10 mL $CHCl_3$ and sonicated for 5 min to remove any unbound polymer chains. The glass slides containing the brush structures were then washed with excess IPA before being blown dry with N_2. The resultant brush films were dried in vacuum for further characterization.

AFM characterization

Atomic force microscopy (AFM) measurements were performed using the PeakForce Quantitative Nanomechanics (QNM) mode on a Bruker Multimode 8 AFM instrument. The

AFM tips were purchased from ScanAsyst Air with a tip radius of 2 nm, a resonance frequency of 70 kHz, and a force constant of 0.4 N/m. The prepared crystals and brush films were dried under vacuum for at least 12 h before imaging. Images of the crystals and brush films were acquired, with a scan size ranging from 3 – 30 μm at a scan speed of 0.8 Hz, for 256 individual lines per image. Image analysis was performed via Bruker Nanoscope Analysis v1.9. 10 different sections were acquired for each observed morphology to calculate average feature height and standard deviation.

Supporting Information

Supporting Information is available from the Wiley Online Library or from the author.

Acknowledgments

This work was supported by the National Science Foundation Grant CHE-1709119 (CYL), CHE-1709663 (BZ), and DMR-2104968 (CYL).

References

[1] a) S. T. Milner, *Science* **1991**, *251*, 905-914; b) W.-L. Chen, R. Cordero, H. Tran, C. K. Ober, *Macromolecules* **2017**, *50*, 4089-4113; c) A. J. Chancellor, B. T. Seymour, B. Zhao, *Anal. Chem.* **2019**, *91*, 6391-6402; d) J. O. Zoppe, N. C. Ataman, P. Mocny, J. Wang, J. Moraes, H. A. Klok, *Chem Rev* **2017**, *117*, 1105-1318; e) B. Li, B. Yu, Q. Ye, F. Zhou, *Acc. Chem. Res.* **2015**, *48*, 229-237; f) R. Barbey, L. Lavanant, D. Paripovic, N. Schuwer, C. Sugnaux, S. Tugulu, H. A. Klok, *Chem Rev* **2009**, *109*, 5437-5527; g) P. Uhlmann, H. Merlitz, J. U. Sommer, M. Stamm, *Macromol. Rapid Commun.* **2009**, *30*, 732-740.

[2] a) B. Zhao, L. Zhu, *Macromolecules* **2009**, *42*, 9369-9383; b) B. Zdyrko, I. Luzinov, *Macromol. Rapid Commun.* **2011**, *32*, 859-869.

[3] a) C. Y. Li, *Polymer* **2020**, *211*, 123150; b) C. Y. Li, *J. Poly. Sci. Poly. Phys.* **2009**, *47*, 2436-2440.

[4] a) S. Mei, M. Staub, C. Y. Li, *Chem. Eur. J.* **2020**, *26*, 349-361; b) M. C. Staub, S. Yu, C. Y. Li, *Giant* **2022**, 100124; c) X. Li, S. Cheng, Y. Zheng, C. Y. Li, *Mol. Sys. Des. Engin.* **2019**, *4*, 793-803; d) S. Cheng, X. Li, Y. Zheng, D. M. Smith, C. Y. Li, *Giant* **2020**, 100021.

[5] a) T. Zhou, H. Qi, L. Han, D. Barbash, C. Y. Li, *Nat. Commun.* **2016**, *7*, 11119; b) S. Mei, C. Y. Li, *Angew Chem Int Ed* **2018**, *57*, 15758-15761; c) T. Zhou, B. Han, H. Qi, Q. Pan, D. M. Smith, L. Han, C. Y. Li, *Nanoscale* **2018**, *10*, 18269-18274; d) S. Mei, J. T. Wilk, A. J. Chancellor, B. Zhao, C. Y. Li, *Macromol. Rap. Commun.* **2020**, 2000228.

[6] a) B. B. Wang, B. Li, B. Zhao, C. Y. Li, *J. Am. Chem. Soc.* **2008**, *130*, 11594-11595; b) B. B. Wang, B. Li, B. Dong, B. Zhao, C. Y. Li, *Macromolecules* **2010**, *43*, 9234-9238; c) B. B. Wang, B. Li, R. C. M. Ferrier, C. Y. Li, *Macromol. Rapid Commun.* **2010**, *31*, 169-175; d) T. Zhou, B. Wang, B. Dong, C. Y. Li, *Macromolecules* **2012**, *45*, 8780-8789; e) T. Zhou, B. Dong, H. Qi, S. Mei, C. Y. Li, *J. Polym. Sci. Poly. Phys.* **2014**, *52*, 1620-1640; f) S. Mei, H. Qi, T. Zhou, C. Y. Li, *Angew. Chem. Inter. Ed.* **2017**, *56*, 13645-13649.

[7] a) P. Geil, *Polymer Single Crystals*, Wiley-lnterscience, **1963**; b) S. Z. D. Cheng, *Phase Transitions in Polymers, the Role of Metastable States*, Elsevier, **2008**; c) B. Wunderlich, *Macromolecular Physics Vol. 1: Crystal Structure, Morphology, Defects*, Academic Press, New York, **1973**; d) H. Qiu, Y. Gao, C. E. Boott, O. E. Gould, R. L. Harniman, M. J. Miles, S. E. Webb, M. A. Winnik, I. Manners, *Science* **2016**, *352*, 697-701; e) M. Inam, J. R. Jones, M. M. Pérez-Madrigal, M. C. Arno, A. P. Dove, R. K. O'Reilly, *ACS Cent. Sci.* **2018**, *4*, 63-70; f) M. C. Staub, S. Kim, S. Yu, C. Y. Li, *ACS Macro Lett.* **2022**, *11*, 1022-1027; g) H. Qi, X. Liu, D. M. Henn, S. Mei, M. C. Staub, B. Zhao, C. Y. Li, *Nat. Commun.* **2020**, *11*, 2152; h) G. R. Burks, H. Qi, S. E. Gleeson, S. Mei, C. Y. Li, *ACS Macro Lett.* **2017**, *7*, 75-79.

[8] a) Y.-X. Liu, E.-Q. Chen, *Coord. Chem. Rev.* **2010**, *254*, 1011-1037; b) B. Lotz, T. Miyoshi, S. Z. Cheng, *Macromolecules* **2017**, *50*, 5995-6025; c) C. Y. Li, J. J. Ge, F. Bai, B. H. Calhoun, F. W. Harris, S. Z. D. Cheng, L. C. Chien, B. Lotz, H. D. Keith, *Macromolecules* **2001**, *34*, 3634-3641; d) G. Reiter, *Chem. Soc. Rev.* **2014**, *43*, 2055-2065; e) G. Reiter, J.-U. Sommer, *Phys. Rev. Lett.* **1998**, *80*, 3771; f) H. Li, S. Yan, *Macromolecules* **2011**, *44*, 417-428; g) J. Xu, Y. Ma, W. Hu, M. Rehahn, G. Reiter, *Nat. Mater.* **2009**, *8*, 348-353.

[9] V. H. Mareau, R. E. Prud'Homme, *Macromolecules* **2005**, *38*, 398-408.

[10] H. Hu, D. L. Dorset, *Macromolecules* **1990**, *23*, 4604-4607.

[11] E. J. Mark, *Polymer Data Handbook*, Oxford University Press, **1999**.

[12] H. Qi, W. Wang, C. Y. Li, *ACS Macro. Lett.* **2014**, *3*, 675-678.

[13] a) C. Sinturel, M. Vayer, M. Morris, M. A. Hillmyer, *Macromolecules* **2013**, *46*, 5399-5415; b) H. M. Aitken, Z. Jiang, I. Hampton, M. L. O'Mara, L. A. Connal, *Mol. Sys. Des. Engin.* **2022**; c) S. Nakagawa, N. Yoshie, *Macromolecules* **2020**, *53*, 8131-8139.

[14] D. S. Boucher, *J. Appl. Polym. Sci.* **2020**, *137*, 48908.

[15] W. Li, C. Bao, R. A. Wright, B. Zhao, *RSC Adv.* **2014**, *4*, 18772-18781.